IOP Publishing New J. Phys. 27 (2025) 023021 https://doi.org/10.1088/1367-2630/adb2b9

New Journal of Physics
The open access journal at the forefront of physics

Deutsche Physikalische Gesellschaft DPG
IOP Institute of Physics

Published in partnership with: Deutsche Physikalische Gesellschaft and the Institute of Physics

OPEN ACCESS

RECEIVED
26 November 2024

REVISED
23 January 2025

ACCEPTED FOR PUBLICATION
5 February 2025

PUBLISHED
13 February 2025

PAPER

Energy boosting and scaling of self-guided hybrid laser-plasma wakefield acceleration in a single uniform plasma

Xinyuan Chang[1,2], **Ming Zeng**[1,2,*], **Jia Wang**[1,2] and **Dazhang Li**[1,2]

[1] Institute of High Energy Physics, Chinese Academy of Sciences, Beijing 100049, People's Republic of China
[2] University of Chinese Academy of Sciences, Beijing 100049, People's Republic of China
[*] Author to whom any correspondence should be addressed.

E-mail: zengming@ihep.ac.cn

Keywords: wakefield accelerator, hybrid laser-plasma wakefield acceleration, beam energy scaling, beam energy boosting

Abstract

In laser-driven plasma wakefield acceleration (LWFA), laser pump depletion and electron dephasing are the major constraints of the electron energy gain. Hybrid laser-PWFA, which uses the laser-accelerated electron beam to drive a beam-driven plasma wakefield in separated stages, has been proposed to increase the beam brightness. However, the overall electron energy gain in hybrid acceleration is even lower than single-stage laser acceleration. In this paper, we report the observation of the energy boosting effect of the hybrid acceleration in single uniform plasmas through a series of particle-in-cell simulations. The self-injected electron beam from the laser-driven wakefield automatically moves forward to drive the beam-driven wakefield after laser depletion. The electrons at the beam tail are then accelerated by the beam-driven plasma wakefield, and the energy gain is at least doubled compared to previous single-stage experiments with the same laser energy. We also propose the scaling of the electron energy gain and the acceleration distance with the laser energy. For example, with a 9.1 J energy laser pulse and a 3.5 cm long plasma of 1.6×10^{18} cm^{-3} density, one can produce a quasi-monoenergetic electron beam at 3.5 GeV energy with 23 pC charge.

1. Introduction

Laser-driven plasma wakefield acceleration (LWFA) [1] and beam-driven plasma wakefield acceleration (PWFA) [2] use the ponderomotive force of intense lasers and the Coulomb force of relativistic electron beams to drive wakefield in plasmas, respectively. In the plasma wakefield, the electrons oscillate around their equilibrium positions, and the much heavier ions are nearly immobile. As a consequence, strong longitudinal electric field and transverse electromagnetic field are generated, which can accelerate and focus electron beams, respectively. Both LWFA and PWFA have been proved as promising mechanisms for accelerating electrons to high energies with the acceleration gradient of the order of 10–100 GeV m^{-1} over recent decades [3–21].

In the single-stage LWFA, two major effects constrain the electron energy gain [22, 23]. One is called the pump-depletion effect, which means the laser is pump depleted after a certain propagation distance due to energy losses in plasma. The other is called the dephasing effect, which means the trapped electrons that approach the speed of light and exceed the phase velocity of the wakefields, outrun the acceleration region and experience the decelerating field. By contrast, the PWFA is ideal for dephasing-free acceleration over much longer distance than the LWFA, capable of doubling the energy gain of the electron driver [7]. But the high peak-current drive beams usually come from large-scale conventional accelerators [24] and are less accessible compared to LWFA.

To gain higher energies, the staged LWFA has been proposed to overcome these two constraints. A common method for the staged LWFA is using multiple separated LWFA stages to extend the acceleration distance [25–30]. However, the staging problems such as the high-divergence effect between stages make it challenging to transport the electron beam. This requires additional spaces for beam optics such as plasma

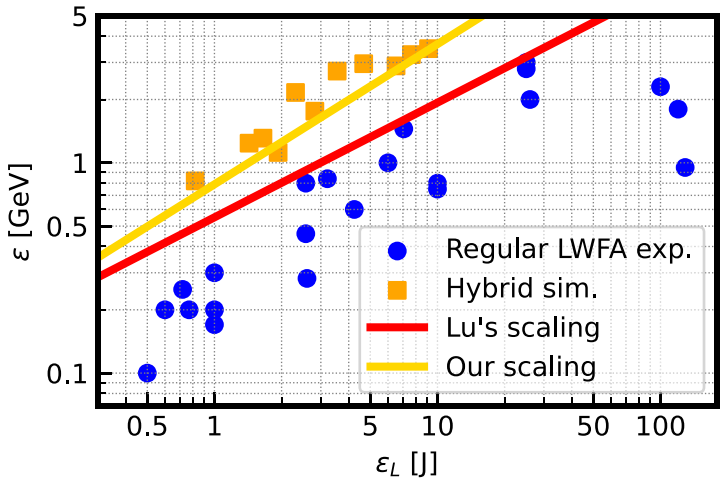

Figure 1. The beam energy gain ε vs drive laser energy ε_L from regular LWFA experiments (blue dots) and single-stage HLPWFA simulations (orange squares). Two scalings are shown for the comparison. Lu's scaling with the maximum energy gain under the self-guided condition equation (14) is shown as the red line, which is the upper-limit of regular LWFA experiments. Our scaling equation (22), based on a phenomenological theory, is shown as the yellow line. The x- and y-axes are in logarithmic scale.

lenses [31–34] to preserve the beam quality, and results in longer footprints, consequently lower averaged acceleration gradients [35]. The staged LWFA can also be realized by the longitudinal density tuning of the plasma, which adds one or more high-density plateaus to the plasma without vacuum gaps [36]. This method has the potential to accelerate electrons to higher energies and enhance the beam quality [37]. However, this method typically uses a plasma channel to effectively guide the laser [38], which introduces extra complexities.

Hybrid laser-PWFA (HLPWFA) uses the LWFA-generated femtosecond scale GeV electron beam with peak current intensity exceeding 10 kA to drive a PWFA [39–46]. It utilizes the advantages of both LWFA and PWFA, and can achieve longer acceleration distance than the pump-depletion and the dephasing lengths of the single-stage LWFA. Recent studies on the hybrid acceleration regulate two separated stages by different plasma densities [47], and reflect the laser at the end of the LWFA by steel foil [48] or block tape [49], and only leave the LWFA-generated electron beam in a vacuum. This electron beam is incident on the second plasma to drive the PWFA, while the trailer is then injected into the wakefield and accelerated from very low energy [50]. The laser reflex process introduces not only staging problems but also a complex experimental setup. Moreover, the trailer in the PWFA stage is newly injected and accelerated from zero energy, and its final energy is not as high as the LWFA generated beam. Instead of an energy booster, recent studies mainly used HLPWFA as a brightness transformer for electron beams [47–53] or a light source [54–56], without much attention devoted to the electron energy gain.

In this paper, we study the HLPWFA in a single uniform plasma over a sufficiently long acceleration distance through particle-in-cell (PIC) simulations. The LWFA creates the self-injected electron beam of the length similar to the plasma wavelength ($\sim$10 μm). The electron beam automatically shifts to the front of the wakefield after laser depletion and drives the PWFA, without requiring of reflecting the laser and using two separated plasma stages. The electrons at the beam tail are then energy boosted due to the PWFA mechanism. This scheme provides a relatively simple setup, avoids staging problems and injection process in the PWFA stage, and concurrently overcomes the two energy constraints of the single-stage LWFA. We propose scaling laws for the electron energy gain and the acceleration distance with the laser energy through theoretical analysis of the excitation of strongly nonlinear plasma wakefields [57], and demonstrate the energy gain is at least doubled compared to previous single-stage self-guided experiments with the same laser energy, as illustrated in figure 1.

The paper is structured as follows. Section 2 shows the simulation observation of the energy boosting effect of the single-stage HLPWFA. Section 3 introduces the energy gain constraints and matching conditions for single-stage self-guided LWFA. Section 4 presents the scaling laws through the phenomenological analysis of wakefields. We summarize our work in section 5.

2. Energy boosting of HLPWFA in uniform plasma

We have used the quasi-3D PIC code FBPIC [58] to simulate the single-stage HLPWFA process. An example simulation is shown in figure 2. In the simulation, the fully-ionized plasma has a 1000 μm long linear

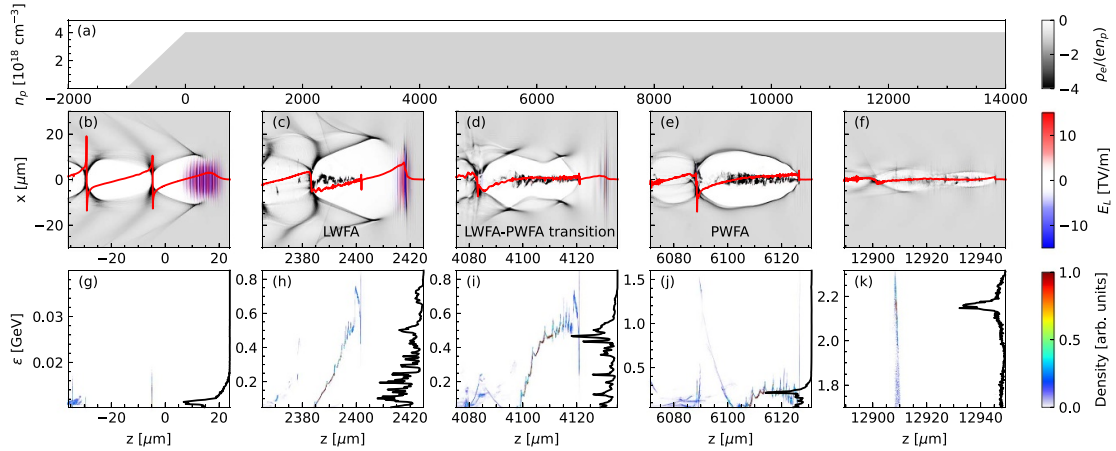

Figure 2. Snapshots of a PIC simulation for a single-stage HLPWFA. (a) The longitudinal plasma profile consists of a 1 mm-long linear upramp and a 14 mm-long flat top. (b)–(f) Density of plasma (gray), laser electric field (red and blue colormap), and the on-axis longitudinal electric field E_z (red line) at different time steps. (g)–(k) The longitudinal phase space density of electrons (rainbow colormap) and the energy spectra (black line) at each corresponding time steps. The focused laser pulse at the start of the flat-top regime (b) creates LWFA (c) before depletion and turns into PWFA (e) after the transition (d), allowing the electrons at the tail accelerated in PWFA (i)–(k). In (b) to (f), the cylindrical coordinate in the simulation has been reconstructed to the Cartesian coordinate, and the slices at $y = 0$ are shown.

upramp, and a half-infinite long flat-top with the density $n_\mathrm{p} = 4 \times 10^{18}\,\mathrm{cm}^{-3}$, as shown in figure 2(a). The simulation uses the cylindrical geometry with two azimuthal modes. The grid sizes are $\Delta z = 0.01 k_\mathrm{p}^{-1}$ and $\Delta r = 0.04 k_\mathrm{p}^{-1}$ in the longitudinal and radial directions, respectively, where $k_\mathrm{p} = \sqrt{4\pi r_\mathrm{e} n_\mathrm{p}}$ is the plasma wavenumber and r_e is the classical electron radius. The number of particles-per-cell is 32. The boundaries of the simulation box are reflective in the r direction and open in the z direction.

In the example, an 800 nm wavelength, 2.3 J energy laser pulse with the focal spot size $w_0 = 11.3\,\mu$m and the duration at full-width-half-maximum (FWHM) $\tau_\mathrm{FWHM} = 25.1$ fs is incident on this plasma, and focused at the start of the flat-top regime of the plasma ($z = 0$). These parameters are chosen under the matching conditions (detailed in section 3) of the laser normalized vector potential amplitude $a_0 = 4.5$ and the peak power $P = 86$ TW. The highly nonlinear wakefield, shown in figures 2(b) and (g), accelerates the self-injected electron beam to high peak current intensity, shown in figures 2(c) and (h). As the laser depletion develops, shown in figures 2(d) and (i), the electron beam automatically shifts to the front of the wakefield and drives the PWFA, shown in figures 2(e) and (j). The electrons at the beam tail are then accelerated by the wakefield in the PWFA until the beam head is almost depleted, substantially exceeding the electron energy gain in the self-guided single-stage LWFA, as shown in figures 2(f) and (k). We refer to this phenomenon as the energy boosting effect. Due to this effect, a quasi-monoenergetic beam with 2.2 GeV energy and 10.9 pC charge can be produced at $z \approx 13$ mm, as shown in figure 2(k). Note that we calculate the summation of the charge within the FWHM range of the monoenergetic peak in the electron spectrum, similar to the method proposed in [59].

We have performed an abundant of simulations with different a_0 and n_p, while w_0 and τ_FWHM satisfies the matching conditions in each of the simulations. Through the simulation results, we find this energy boosting effect occurs after a sufficiently long acceleration distance if a_0 is between 3.5 and 5. For $a_0 < 3.5$, the self-injected beam has too few charge to drive the PWFA efficiently. And for $a_0 > 5$, the electrons do not gain high enough energy in the LWFA. A good trade off between the beam charge and the beam energy is found at $a_0 \approx 4.5$. Thus, we have scanned n_p with fixed $a_0 = 4.5$, with the results shown as the orange squares in figure 1. For example, a 4.7 J energy laser pulse interacts with a plasma of density $n_\mathrm{p} = 2.5 \times 10^{18}\,\mathrm{cm}^{-3}$ (thus, $w_0 = 14.3\,\mu$m and $\tau_\mathrm{FWHM} = 31.7$ fs according to the matching conditions), and produces a quasi-monoenergetic beam with 3.0 GeV energy and 15 pC charge at $z \approx 18$ mm. This energy gain is five-fold the regular LWFA experimental result in [60] with the same drive laser energy, and nearly doubled the optimized LWFA experimental result in [21] with the same drive laser energy. In another example, a 9.1 J energy laser pulse interacts with a plasma of density $n_p = 1.6 \times 10^{18}\,\mathrm{cm}^{-3}$ (thus, $w_0 = 17.8\,\mu$m and $\tau_\mathrm{FWHM} = 39.6$ fs according to the matching conditions), and produces a quasi-monoenergetic beam with 3.5 GeV energy and 23 pC charge at $z \approx 35$ mm, quadrupling the experimental results with the same drive laser energy, for 0.8 GeV energy gain in [61] and 0.75 GeV energy gain in [62]. The energy evolution of the peak electron energy for the beam head and for the beam tail in the three aforementioned cases is shown in figure 3.

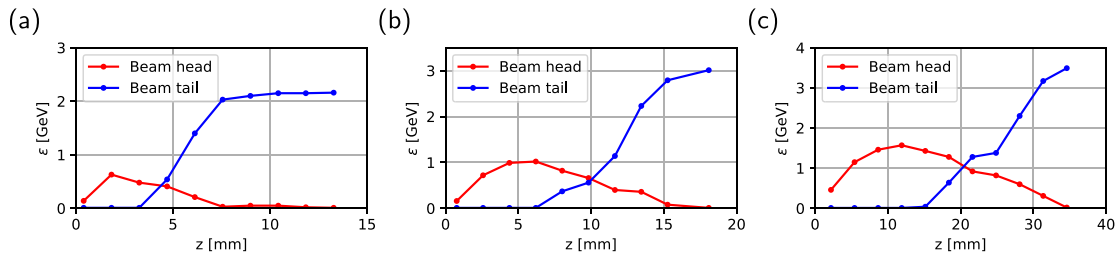

Figure 3. The evolution of the peak energy for the beam head (red) and for the beam tail (blue) in three cases: (a) $a_0 = 4.5$ and $n_p = 4.0 \times 10^{18}$ cm^{-3}; (b) $a_0 = 4.5$ and $n_p = 2.5 \times 10^{18}$ cm^{-3}; (c) $a_0 = 4.5$ and $n_p = 1.6 \times 10^{18}$ cm^{-3}. The LWFA generates and accelerates a high-current electron beam to the energy of the order of 1 GeV. After the laser is depleted, through the PWFA mechanism, the head of the electron beam transfer its energy to the tail of the beam, which is then accelerated to several GeVs.

Note that the single-stage HLPWFA was previously mentioned by Pae *et al* [40], but the transverse grid size in their simulation was too large to show the high-energy quasi-monoenergetic beam (we have reproduced their result with their grid size). Also in Masson-Laborde *et al* [41], the relatively small choice of a_0 ($\sim$1.7) and the large choice of n_p ($\sim 10^{19}$ cm^{-3}), which are not suitable for the energy boosting effect, resulted in a short effective acceleration distance and low energy gain of the beam.

3. Theory for self-guided single-stage LWFA

For a single-stage LWFA, the peak accelerating fields can be estimated by $E_{z,\max} = \sqrt{a_0} m_e c \omega_p / e$, where $a_0 \equiv eE_0/(m_e \omega_0 c)$ is the peak normalized vector potential of the laser, e is the elementary charge, E_0 is the peak amplitude of the laser electric field, m_e is the rest mass of electron, $\omega_0 = 2\pi c/\lambda_0$ is the laser frequency, c is the speed of light in vacuum, λ_0 is the laser wavelength and $\omega_p = ck_p$ is the plasma frequency [22]. The laser focal spot size w_0 needs to be matched to the blowout radius R for the most ideal wake as [22]

$$R \simeq w_0 = \frac{2\sqrt{a_0}}{k_p}. \tag{1}$$

As mentioned in section 1, the drive laser is pump depleted after the pump depletion length [22, 23]

$$L_{pd} \simeq \left(\frac{\omega_0}{\omega_p}\right)^2 c\tau_{FWHM}. \tag{2}$$

The trapped electrons accelerated beyond the phase velocity of the wakefields outrun the acceleration region after the dephasing length [22]

$$L_{dp} \simeq \frac{2}{3}\left(\frac{\omega_0}{\omega_p}\right)^2 R. \tag{3}$$

The condition for $L_{pd} = L_{dp}$ is

$$c\tau_{FWHM} = \frac{2}{3}R. \tag{4}$$

Equations (1) and (4) are referred to as the matching conditions for the single-stage LWFA.

The energy of a laser pulse with the Gaussian temporal profile can be calculated as

$$\varepsilon_L = \frac{1}{2}\sqrt{\frac{\pi}{\ln 2}} P \tau_{FWHM}, \tag{5}$$

where $P = (\pi^2 m_e c^3 a_0^2 w_0^2)/(4 r_e \lambda_0^2)$ is the peak power of the laser pulse. The pulse energy of the laser under the matching conditions can be determined by a_0 and n_p as

$$\varepsilon_L = \frac{\pi}{12\sqrt{\ln 2}} \frac{a_0^{\frac{7}{2}}}{r_e^{\frac{5}{2}} \lambda_0^2 n_p^{\frac{3}{2}}} m_e c^2. \tag{6}$$

We rewrite equation (6) to express the plasma density by a_0 and ε_L,

$$n_{\rm p} = \left(\frac{\pi}{12\sqrt{\ln 2}}\right)^{\frac{2}{3}} \left(\frac{m_{\rm e}c^2}{\varepsilon_L}\right)^{\frac{2}{3}} \frac{a_0^{\frac{7}{3}}}{r_{\rm e}^{\frac{5}{3}}\lambda_0^{\frac{4}{3}}}, \tag{7}$$

or

$$n_{\rm p}\ \left[{\rm cm}^{-3}\right] \approx 0.21\times 10^{18}\left(\frac{1}{\varepsilon_L\ [{\rm J}]}\right)^{\frac{2}{3}}\left(\frac{0.8}{\lambda_0\ [\mu{\rm m}]}\right)^{\frac{4}{3}} a_0^{\frac{7}{3}}. \tag{8}$$

For the self-guided LWFA [60–67], the diffraction of the laser pulse is balanced by the relativistic and ponderomotive self-focusing effects [68], without the external guiding such as plasma waveguides [69]. In this case, another condition needs to be fulfilled for the self-guiding to occur, as [22]

$$a_0 \gtrsim \left(\frac{n_{\rm c}}{n_{\rm p}}\right)^{\frac{1}{5}}, \tag{9}$$

where $n_{\rm c} = \omega_0^2/(4\pi r_{\rm e}c^2)$ is the critical density. We derive the minimum plasma density for the self-guided LWFA through equations (7) and (9),

$$n_{\rm s} = \frac{\pi^{\frac{17}{22}}}{\left(12\sqrt{\ln 2}\right)^{\frac{5}{11}}}\left(\frac{m_{\rm e}c^2}{\varepsilon_L}\right)^{\frac{5}{11}} r_{\rm e}^{-\frac{16}{11}}\lambda_0^{-\frac{17}{11}}, \tag{10}$$

or

$$n_{\rm s}\ \left[{\rm cm}^{-3}\right] \approx 3.69\times 10^{18}\left(\frac{1}{\varepsilon_L\ [{\rm J}]}\right)^{\frac{5}{11}}\left(\frac{0.8}{\lambda_0\ [\mu{\rm m}]}\right)^{\frac{17}{11}}. \tag{11}$$

The maximum energy gain for self-injected electrons in the nonlinear self-guided LWFA is achieved with the minimum plasma density $n_{\rm s}$, and satisfies [22]

$$\varepsilon_{\rm max} = \frac{2}{3}\frac{n_{\rm c}}{n_{\rm s}} a_0 m_{\rm e}c^2. \tag{12}$$

We use equations (9), (10) and (12) to derive the maximum energy gain of the electrons as a function of the drive laser energy as

$$\varepsilon_{\rm max} = \frac{2}{3}\left(\frac{12 r_{\rm e}\sqrt{\pi\ln 2}}{\lambda_0}\right)^{\frac{6}{11}} \varepsilon_L^{\frac{6}{11}}\left(m_{\rm e}c^2\right)^{\frac{5}{11}}, \tag{13}$$

or

$$\varepsilon_{\rm max}\ [{\rm GeV}] \approx 0.55\left(\frac{0.8}{\lambda_0\ [\mu{\rm m}]}\right)^{\frac{6}{11}} \varepsilon_L^{\frac{6}{11}}\ [{\rm J}]. \tag{14}$$

For $\lambda_0 = 0.8\,\mu$m, this scaling is shown as the red line in figure 1.

We present plenty of self-guided LWFA experimental results [3–6, 10–13, 15, 16, 18, 25–27, 60–62, 66, 67] as the blue dots in figure 1. Note that equation (14) is the upper limit of the electron energy gain in regular self-guided LWFAs.

4. A phenomenological energy boosting theory and our scaling

To find the energy boosting ratio and the energy transformer ratio in the PWFA, we need to know the deceleration field of the electron beam head and the acceleration field of the electron beam tail. We consider the normalized current distribution $\Lambda(\xi) = \int_0^\infty n_{\rm B}(\xi, r) r{\rm d}r$ of the LWFA-generated electron beam, where $n_{\rm B}$ is the electron beam density normalized to $n_{\rm p}$, $\xi = k_{\rm p}(ct - z)$ is in the normalized co-moving coordinate, and r is the radial coordinate normalized to $k_{\rm p}^{-1}$. $\Lambda(\xi)$ also satisfies $\Lambda(\xi) = 2I(\xi)/I_A$, where $I(\xi)$ is the current distribution, and $I_A = ec/r_{\rm e} \approx 17$ kA is the Alfvén current. An example of the distribution of Λ is shown in figure 4(a). The head of the electron beam can be modeled to have a triangular distribution with the peak of

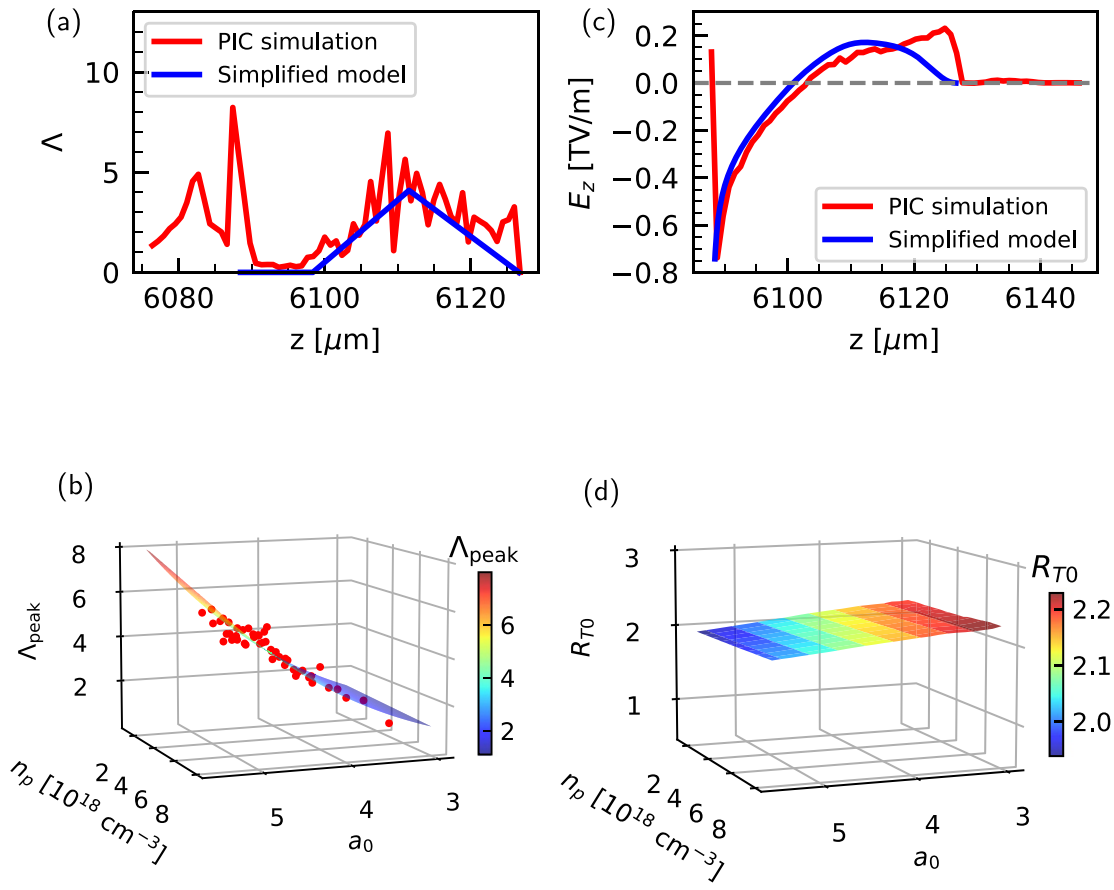

Figure 4. Current density, longitudinal electric field and instant transformer ratio distribution from PIC simulations and our model. (a) The normalized current distribution Λ of one PIC simulation example (red line) and of the simplified triangular model (blue line). (b) The peak current of the head of the electron beam Λ_{peak} in simulations with different a_0 and n_p (red dots), and the fit equation (15) is shown as the colored surface. (c) The longitudinal electric field distribution E_z from the example PIC simulation (red line) and from solving equations (16) and (17) based on the simplified triangular model of Λ (blue line). (d) The instant transformer ratio with different a_0 and n_p based on our simplified model. In all cases, we have $\Lambda_{peak} > 1.35$ (and consequently $I_{peak} > 11.5$ kA).

Λ_{peak} and the length of $L_B \approx 5R/2 \approx 5w_0/2$. Through a series of simulations with different a_0 and n_p, we fit Λ_{peak} by

$$\Lambda_{peak} \simeq \left(0.0492 - 0.0013 \times \frac{n_p}{10^{18}\ \mathrm{cm}^{-3}}\right) a_0^3, \tag{15}$$

as shown in figure 4(b).

With the modeled distribution of Λ, the blowout radius r_b, normalized to k_p^{-1}, can be numerically calculated by [57, 70–72]

$$\left(\frac{r_b^3}{4} + r_b\right)\frac{d^2 r_b}{d\xi^2} + \left(1 + \frac{r_b^2}{2}\right)\left(\frac{dr_b}{d\xi}\right)^2 + \frac{r_b^2}{4} = \Lambda, \tag{16}$$

and the longitudinal electric field E_z, normalized to $m_e c\omega_p/e$, can be calculated by

$$E_z = \frac{1}{2} r_b \frac{dr_b}{d\xi}. \tag{17}$$

The comparison of the simulated longitudinal electric field and the model-calculated one, for the case of figure 2(e), is plotted in figure 4(c) and shows good agreement. Note that the numerical calculation should terminate at the closure of the blowout, where $r_b = 0$ and E_z reaches minimum.

After the E_z distribution is obtained, one may calculate the averaged acceleration and deceleration fields $\bar{E}_{acc}$ and $\bar{E}_{dec}$, which are the $E_z < 0$ and $E_z > 0$ parts averaged along ξ, respectively. The instant energy transformer ratio [73], defined as $R_{T0} \equiv -\bar{E}_{acc}/\bar{E}_{dec}$, can be numerically calculated according to equations (15), (16) and (17) with different parameters of a_0 and n_p, which is plotted in figure 4(d). We can

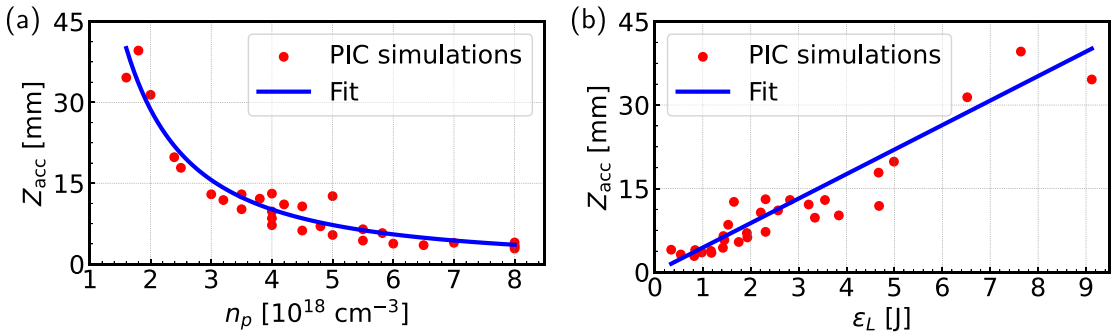

Figure 5. (a) The acceleration distances Z_{acc} vs plasma density n_p for $3.5 < a_0 < 5$ (red dots), and the fit equation (23) by asserting $a_0 = 4.5$ (blue line). (b) The scaling of the acceleration distance with the laser energy equation (25) (blue line) compared with the simulation results (red dots).

see that $R_{T0} \simeq 2.1 \pm 0.1$ is a good approximation for a relatively broad range of $3.5 < a_0 < 5$ and 1.5×10^{18} cm$^{-3} < n_p < 8 \times 10^{18}$ cm^{-3}.

The energy of the electron beam after the LWFA can be estimated by the original version of Lu's scaling [22]

$$\varepsilon_{\rm LWFA} = \frac{2}{3}\frac{n_c}{n_p} a_0 m_e c^2. \tag{18}$$

After the PWFA, the head of the electron beam looses all the energy, and the tail of the electron beam is boosted to the energy of ε. The overall energy transformer ratio, which is approximately half of the instant energy transformer ratio, can be written as

$$R_T = \frac{\varepsilon - \varepsilon_{\rm LWFA}}{\varepsilon_{\rm LWFA} - 0} = \frac{1}{2} R_{T0}. \tag{19}$$

This leads to the boosted energy of

$$\varepsilon = \frac{2}{3}\left(\frac{1}{2}R_{T0} + 1\right)\frac{n_c}{n_p} a_0 m_e c^2. \tag{20}$$

We use equations (7) and (20) to rewrite the boosted energy as

$$\varepsilon = \frac{4}{3}\left(\frac{1}{2}R_{T0} + 1\right)(18\pi \ln 2)^{\frac{1}{3}} a_0^{-\frac{4}{3}} \left(\frac{r_e}{\lambda_0}\right)^{\frac{2}{3}} \left(m_e c^2 \varepsilon_L^2\right)^{\frac{1}{3}}. \tag{21}$$

Note a_0 is not arbitrary in our model. As mentioned before, $3.5 < a_0 < 5$ is required for the effective energy boosting, and $a_0 \approx 4.5$ is a good trade off between the beam charge and the beam energy. We see in figure 4(d) that R_{T0} decreases with a_0, and $R_{T0} \approx 2.1$ for $a_0 \approx 4.5$. Thus, we take $R_{T0} = 2.1$ and $a_0 = 4.5$, and our scaling for the boosted energy is obtained as

$$\varepsilon\ [\rm GeV] = 0.79\left(\frac{0.8}{\lambda_0\ [\mu\rm m]}\varepsilon_L\ [\rm J]\right)^{\frac{2}{3}}. \tag{22}$$

The scaling with the commonly used $\lambda_0 = 0.8\ \mu$m is plotted in figure 1 as the yellow line, to compare with the single-stage HLPWFA simulations described in section 2. One can see that our scaling reasonably illustrates the energy boosting of the hybrid acceleration.

Another critical problem of the hybrid acceleration is the total acceleration distance Z_{acc}, at which the head of the electron beam looses all the energy and the tail of the electron beam does not gain energy anymore. To study this, we plot Z_{acc} vs n_p in figure 5(a) as the red dots, while different a_0 cases within the range $3.5 < a_0 < 5$ are collected in the same plot. We find that Z_{acc} mainly depends on n_p, but is not sensitive to a_0. We use a similar acceleration distance scaling as Shadwick *et al* [23], but with a different prefactor obtained by fit

$$Z_{acc} = 7.8\left(1 + \frac{2}{a_0^2}\right)\frac{n_c}{n_p} k_p^{-1}. \tag{23}$$

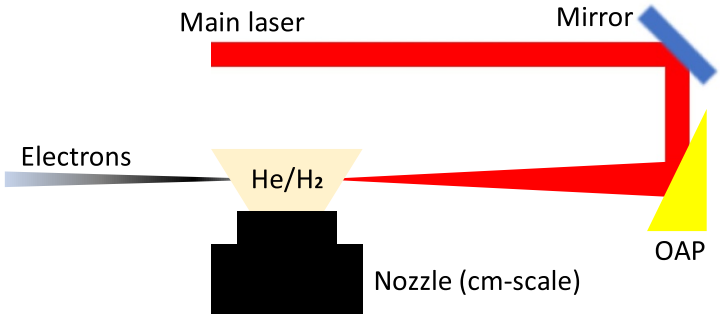

Figure 6. A possible experimental setup for the HLPWFA in a single uniform plasma. A high-power laser beam is focused in vacuum by an off-axis parabolic (OAP) mirror at the front edge of the low-Z gas ejected from the nozzle. The low-Z gas, such as helium or hydrogen, is ionized by the laser prepulse or the remnant of the laser after pump-depletion, to form the plasma target. Both the LWFA and PWFA processes occur in the same plasma target, and energy boosted electrons are generated at the rear side of the plasma target. The opening of the nozzle should be wide enough to support the acceleration distance, which scales as equation (25). The proper f-number of the OAP mirror can be estimated according to $F \approx 1.2 w_0/\lambda_0$.

We assert $a_0 = 4.5$ once more, and plot this fit in figure 5(a) as the blue line, which shows good agreement with the simulation results. As a comparison, the acceleration distance of a regular LWFA under the matching conditions, which is the pump depletion length and the dephasing length $L_{\rm pd} = L_{\rm dp} = \frac{4}{3}\sqrt{a_0} n_{\rm c} n_{\rm p}^{-1} k_{\rm p}^{-1}$ according to equations (1)–(4), is only about 1/3 of $Z_{\rm acc}$ for $a_0 = 4.5$.

To further obtain the $Z_{\rm acc}$ scaling with the laser energy, we use equations (7) and (23) to write

$$Z_{\rm acc} \simeq 46.8 \sqrt{\frac{\ln 2}{\pi}} \left(1 + \frac{2}{a_0^2}\right) a_0^{-\frac{7}{2}} \left(\frac{\varepsilon_L}{m_{\rm e} c^2}\right) r_{\rm e}, \tag{24}$$

which is simplified to

$$Z_{\rm acc}\ [\rm mm] \simeq 4.40 \varepsilon_L\ [\rm J]\,, \tag{25}$$

if we assert $a_0 = 4.5$. This acceleration distance scaling is shown in figure 5(b) as the blue line, which has good agreement with the simulations shown as the red dots.

5. Conclusion

We have observed the energy boosting effect in the HLPWFA in a single uniform plasma, as the energy of the tail of the LWFA-generated electron beam can be further accelerated in the PWFA, which concurrently overcome the two major constraints on the electron energy gain of the regular single-stage LWFA. We have also proposed the scaling for the electron energy gain equation (22) and the acceleration distance equation (25), as functions of the drive laser energy based on a phenomenological theory. It is found that the HLPWFA has the potential to at least double the energy gain compared to previous regular self-guided LWFA experiments using the same energy drive laser. Meanwhile, this concept has the potential to become a novel solution for EuPRAXIA [44, 45]. The energy boosting effect and scaling of the HLPWFA can be experimentally examined with a common LWFA setup, illustrated in figure 6, if proper parameters are chosen.

The simulations were performed on a single NVIDIA A100 GPU with 40 GB memory. The computation time for one simulation ranges from 28 to 44 h, depending on the simulation parameters. It should be noted that the simulation with a plasma density lower than 1×10^{18} cm^{-3} cannot be performed with an adequate grid resolution, because of the memory capacity limitation. Nevertheless, our scaling suggests that the similar energy boosting effect can occur with lower densities, and consequently larger laser energies according to equation (7).

Data availability statement

All data that support the findings of this study are included within the article (and any supplementary files).

Acknowledgments

This work is supported by the Strategic Priority Research Program of the Chinese Academy of Sciences (Grant No. XDB0530000) and the National Natural Science Foundation of China (Grant No. 12475159).

ORCID iDs

Xinyuan Chang https://orcid.org/0009-0000-1031-7245
Ming Zeng https://orcid.org/0000-0002-1357-640X
Jia Wang https://orcid.org/0000-0003-2341-5201
Dazhang Li https://orcid.org/0000-0001-6412-8853

References

[1] Tajima T and Dawson J M 1979 Laser electron accelerator *Phys. Rev. Lett.* **43** 267
[2] Chen P, Dawson J M, Huff R W and Katsouleas T 1985 Acceleration of electrons by the interaction of a bunched electron beam with a plasma *Phys. Rev. Lett.* **55** 1537
[3] Malka V *et al* 2002 Electron acceleration by a wake field forced by an intense ultrashort laser pulse *Science* **298** 1596
[4] Faure J, Glinec Y, Pukhov A, Kiselev S, Gordienko S, Lefebvre E, Rousseau J P, Burgy F and Malka V 2004 A laser-plasma accelerator producing monoenergetic electron beams *Nature* **431** 541
[5] Mangles S P D *et al* 2004 Monoenergetic beams of relativistic electrons from intense laser-plasma interactions *Nature* **431** 535
[6] Faure J, Rechatin C, Norlin A, Lifschitz A, Glinec Y and Malka V 2006 Controlled injection and acceleration of electrons in plasma wakefields by colliding laser pulses *Nature* **444** 737
[7] Blumenfeld I *et al* 2007 Energy doubling of 42 GeV electrons in a metre-scale plasma wakefield accelerator *Nature* **445** 741
[8] Tzoufras M, Lu W, Tsung F, Huang C, Mori W, Katsouleas T, Vieira J, Fonseca R and Silva L 2008 Beam loading in the nonlinear regime of plasma-based acceleration *Phys. Rev. Lett.* **101** 145002
[9] Kalmykov S, Yi S A, Khudik V and Shvets G 2009 Electron self-injection and trapping into an evolving plasma bubble *Phys. Rev. Lett.* **103** 135004
[10] Buck A *et al* 2013 Shock-front injector for high-quality laser-plasma acceleration *Phys. Rev. Lett.* **110** 185006
[11] Corde S, Thaury C, Lifschitz A, Lambert G, Ta Phuoc K, Davoine X, Lehe R, Douillet D, Rousse A and Malka V 2013 Observation of longitudinal and transverse self-injections in laser-plasma accelerators *Nat. Commun.* **4** 1501
[12] Wang X *et al* 2013 Quasi-monoenergetic laser-plasma acceleration of electrons to 2 GeV *Nat. Commun.* **4** 1988
[13] Wang W T *et al* 2016 High-brightness high-energy electron beams from a laser wakefield accelerator via energy chirp control *Phys. Rev. Lett.* **117** 124801
[14] Couperus J P *et al* 2017 Demonstration of a beam loaded nanocoulomb-class laser wakefield accelerator *Nat. Commun.* **8** 487
[15] Ke L T *et al* 2021 Near-GeV electron beams at a few per-mille level from a laser wakefield accelerator via density-tailored plasma *Phys. Rev. Lett.* **126** 214801
[16] Kirchen M *et al* 2021 Optimal beam loading in a laser-plasma accelerator *Phys. Rev. Lett.* **126** 174801
[17] Peña F *et al* 2024 Energy depletion and re-acceleration of driver electrons in a plasma-wakefield accelerator *Phys. Rev. Res.* **6** 043090
[18] Grafenstein K V *et al* 2023 Laser-accelerated electron beams at 1 GeV using optically-induced shock injection *Sci. Rep.* **13** 11680
[19] Xu X, Dalichaouch T, Liu J, Qianyi M, Pierce J, Miller K, Yan X and Mori W 2023 Generation of ultrabright and low energy spread electron beams in laser wakefield acceleration in a uniform plasma *Phys. Rev. Accel. Beams* **26** 111302
[20] Aniculaesei C *et al* 2023 The acceleration of a high-charge electron bunch to 10 GeV in a 10-cm nanoparticle-assisted wakefield accelerator *Matter Radiat. Extremes* **9** 014001
[21] Põder K *et al* 2024 Multi-GeV electron acceleration in wakefields strongly driven by oversized laser spots *Phys. Rev. Lett.* **132** 195001
[22] Lu W, Tzoufras M, Joshi C, Tsung F, Mori W, Vieira J, Fonseca R and Silva L 2007 Generating multi-GeV electron bunches using single stage laser wakefield acceleration in a 3d nonlinear regime *Phys. Rev. Spec. Top. Accel. Beams* **10** 061301
[23] Shadwick B A, Schroeder C B and Esarey E 2009 Nonlinear laser energy depletion in laser-plasma acceleratorsa) *Phys. Plasmas* **16** 056704
[24] Hogan M J *et al* 2010 Plasma wakefield acceleration experiments at facet *New J. Phys.* **12** 055030
[25] Pollock B B *et al* 2011 Demonstration of a narrow energy spread, approximately 0.5 GeV electron beam from a two-stage laser wakefield accelerator *Phys. Rev. Lett.* **107** 045001
[26] Liu J S *et al* 2011 All-optical cascaded laser wakefield accelerator using ionization-induced injection *Phys. Rev. Lett.* **107** 035001
[27] Kim H T, Pae K H, Cha H J, Kim I J, Yu T J, Sung J H, Lee S K, Jeong T M and Lee J 2013 Enhancement of electron energy to the multi-GeV regime by a dual-stage laser-wakefield accelerator pumped by petawatt laser pulses *Phys. Rev. Lett.* **111** 165002
[28] Steinke S *et al* 2016 Multistage coupling of independent laser-plasma accelerators *Nature* **530** 190
[29] Luo J *et al* 2018 Multistage coupling of laser-wakefield accelerators with curved plasma channels *Phys. Rev. Lett.* **120** 154801
[30] Pathak V B, Kim H T, Vieira J, Silva L O and Nam C H 2018 All optical dual stage laser wakefield acceleration driven by two-color laser pulses *Sci. Rep.* **8** 11772
[31] Thaury C *et al* 2014 Demonstration of relativistic electron beam focusing by a laser-plasma lens *Nat. Commun.* **6** 6860
[32] Kuschel S *et al* 2016 Demonstration of passive plasma lensing of a laser wakefield accelerated electron bunch *Phys. Rev. Accel. Beams* **19** 071301
[33] Thaury C *et al* 2007 Plasma mirrors for ultrahigh-intensity optics *Nat. Phys.* **3** 424
[34] Ferran Pousa A, Martinez de la Ossa A, Brinkmann R and Assmann R W 2019 Compact multistage plasma-based accelerator design for correlated energy spread compensation *Phys. Rev. Lett.* **123** 054801
[35] Lindstrøm C A 2021 Staging of plasma-wakefield accelerators *Phys. Rev. Accel. Beams* **24** 014801
[36] Zhu X-L, Chen M, Weng S-M, Yu T-P, Wang W-M, He F, Sheng Z-M, McKenna P, Jaroszynski D A and Zhang J 2020 Extremely brilliant GeV Y-rays from a two-stage laser-plasma accelerator *Sci. Adv.* **6** eaaz7240
[37] Liu S, Li F, Zhou S, Hua J, Mori W, Joshi C and Lu W 2024 A scalable, high-efficiency, low-energy-spread, laser wakefield accelerator using a tri-plateau plasma channel *Research* **7** 0396
[38] Kim J U, Hafz N and Suk H 2004 Electron trapping and acceleration across a parabolic plasma density profile *Phys. Rev.* E **69** 026409
[39] Hidding B, Königstein T, Osterholz J, Karsch S, Willi O and Pretzler G 2010 Monoenergetic energy doubling in a hybrid laser-plasma wakefield accelerator *Phys. Rev. Lett.* **104** 195002
[40] Pae K, Choi I and Lee J 2010 Self-mode-transition from laser wakefield accelerator to plasma wakefield accelerator of laser-driven plasma-based electron acceleration *Phys. Plasmas* **17** 123104

[41] Masson-Laborde P E, Mo M Z, Ali A, Fourmaux S, Lassonde P, Kieffer J C, Rozmus W, Teychenné D and Fedosejevs R 2014 Giga-electronvolt electrons due to a transition from laser wakefield acceleration to plasma wakefield acceleration *Phys. Plasmas* **21** 123113
[42] Guillaume E *et al* 2015 Physics of fully-loaded laser-plasma accelerators *Phys. Rev. Spec. Top. Accel. Beams* **18** 061301
[43] Chou S-W, Xu J, Khrennikov K, Cárdenas D, Wenz J, Heigoldt M, Hofmann L, Veisz L and Karsch S 2016 Collective deceleration of laser-driven electron bunches *Phys. Rev. Lett.* **117** 144801
[44] Walker P A *et al* 2017 Horizon 2020 eupraxia design study *J. Phys.: Conf. Ser.* **874** 012029
[45] Assmann R W *et al* 2020 Eupraxia conceptual design report *Eur. Phys. J. Spec. Top.* **229** 3675
[46] Wan Y, Tata S, Seemann O, Levine E Y, Kroupp E and Malka V 2024 Real-time visualization of the laser-plasma wakefield dynamics *Sci. Adv.* **10** eadj3595
[47] Martinez de la Ossa A *et al* 2019 Hybrid lwfa-pwfa staging as a beam energy and brightness transformer: conceptual design and simulations *Phil. Trans. R. Soc.* A **377** 20180175
[48] Kurz T *et al* 2021 Demonstration of a compact plasma accelerator powered by laser-accelerated electron beams *Nat. Commun.* **12** 2895
[49] Foerster F M *et al* 2022 Stable and high-quality electron beams from staged laser and plasma wakefield accelerators *Phys. Rev.* X **12** 041016
[50] Hidding B *et al* 2023 Progress in hybrid plasma wakefield acceleration *Photonics* **10** 99
[51] Heinemann T *et al* 2017 Investigating the key parameters of a staged laser- and particle driven plasma wakefield accelerator experiment *Int. Particle Accelerator Conf. (8th), IPAC2017* (JACoW) p TUIK010
[52] Hidding B *et al* 2019 Fundamentals and applications of hybrid lwfa-pwfa *Appl. Sci.* **9** 2626
[53] Götzfried J *et al* 2020 Physics of high-charge electron beams in laser-plasma wakefields *Phys. Rev.* X **10** 041015
[54] Holloway J A, Norreys P A, Thomas A G R, Bartolini R, Bingham R, Nydell J, Trines R, Walker R and Wing M 2017 Brilliant x-rays using a two-stage plasma insertion device *Sci. Rep.* **7** 3985
[55] Ferri J *et al* 2017 High-brilliance betatron gamma-ray source powered by laser-accelerated electrons *Phys. Rev. Lett.* **120** 254802
[56] Dong C, Zhao T, Behm K, Cummings P, Nees J, Maksimchuk A, Yanovsky V, Krushelnick K and Thomas A 2018 High flux femtosecond x-ray emission from the electron-hose instability in laser wakefield accelerators *Phys. Rev. Spec. Top. Accel. Beams* **21** 041303
[57] Golovanov A, Kostyukov I Y, Pukhov A and Malka V 2023 Energy-conserving theory of the blowout regime of plasma wakefield *Phys. Rev. Lett.* **130** 105001
[58] Lehe R, Kirchen M, Andriyash I A, Godfrey B B and Vay J-L 2016 A spectral, quasi-cylindrical and dispersion-free Particle-In-Cell algorithm *Comput. Phys. Commun.* **203** 66
[59] Zeng M 2024 Simulation observation of high effectiveness laser plasma wakefield accelerator using plasma telescope configuration *Phys. Plasmas* **31** 080702
[60] Clayton C E *et al* 2010 Self-guided laser wakefield acceleration beyond 1 GeV using ionization-induced injection *Phys. Rev. Lett.* **105** 105003
[61] Froula D H *et al* 2009 Measurements of the critical power for self-injection of electrons in a laser wakefield accelerator *Phys. Rev. Lett.* **103** 215006
[62] Kneip S *et al* 2009 Near-GeV acceleration of electrons by a nonlinear plasma wave driven by a self-guided laser pulse *Phys. Rev. Lett.* **103** 035002
[63] Ralph J E *et al* 2010 Laser wakefield acceleration at reduced density in the self-guided regime *Phys. Plasmas* **17** 056709
[64] Davidson A, tableman A, Yu P, An W, Tsung F, Lu W, Fonseca R A and Mori W B 2017 An examination of the scaling laws for LWFA in the self-guided nonlinear blowout regime *AIP Conf. Proc.* **1812** 040014
[65] Joshi C 2017 Laser-driven plasma accelerators operating in the self-guided, blowout regime *IEEE Trans. Plasma Sci.* **45** 3134
[66] Kim H T *et al* 2017 Stable multi-GeV electron accelerator driven by waveform-controlled pw laser pulses *Sci. Rep.* **7** 10203
[67] Shin J *et al* 2018 Quasi-monoenergetic multi-GeV electron acceleration by optimizing the spatial and spectral phases of pw laser pulses *Plasma Phys. Control. Fusion* **60** 064007
[68] Sun G, Ott E, Lee Y and Guzdar P 1987 Self-focusing of short intense pulses in plasmas *Phys. Fluids* **30** 526
[69] Gonsalves A J *et al* 2019 Petawatt laser guiding and electron beam acceleration to 8 GeV in a laser-heated capillary discharge waveguide *Phys. Rev. Lett.* **122** 084801
[70] Lu W, Huang C, Zhou M, Tzoufras M, Tsung F S, Mori W B and Katsouleas T 2006 A nonlinear theory for multidimensional relativistic plasma wave wakefieldsa) *Phys. Plasmas* **13** 056709
[71] Lu W, Huang C, Zhou M, Mori W B and Katsouleas T 2006 Nonlinear theory for relativistic plasma wakefields in the blowout regime *Phys. Rev. Lett.* **96** 165002
[72] Golovanov A, Kostyukov I, Reichwein L, Thomas J and Pukhov A 2021 Excitation of strongly nonlinear plasma wakefield by electron bunches *Plasma Phys. Control. Fusion* **63** 085004
[73] Lu W, An W, Huang C, Joshi C, Mori W, Hogan M, Raubenheimer T and Seryi A 2010 High transformer ratio PWFA for application on XFELs *Part. Accel. Conf.* WE6RFP098